ACS OMEGA

http://pubs.acs.org/journal/acsodf

Article

Improving the Performance and Stability of Perovskite Light-Emitting Diodes by a Polymeric Nanothick Interlayer-Assisted Grain Control Process

Loganathan Veeramuthu,[‖] Fang-Cheng Liang,[‖] Zhi-Xuan Zhang, Chia-Jung Cho, Ender Ercan, Chu-Chen Chueh, Wen-Chang Chen, Redouane Borsali, and Chi-Ching Kuo*

Cite This: *ACS Omega* 2020, 5, 8972−8981

Read Online

ACCESS | Metrics & More | Article Recommendations | Supporting Information

ABSTRACT: $CsPbBr_3$ is a promising light-emitting material due to its wet solution processability, high photoluminescence quantum yield (PLQY), narrow color spectrum, and cost-effectiveness. Despite such advantages, the morphological defects, unsatisfactory carrier injection, and stability issues retard its widespread applications in light-emitting devices (LEDs). In this work, we demonstrated a facile and cost-effective method to improve the morphology, efficiency, and stability of the $CsPbBr_3$ emissive layer using a dual polymeric encapsulation governed by an interface-assisted grain control process (IAGCP). An eco-friendly low-cost hydrophilic polymer poly(vinylpyrrolidone) (PVP) was blended into the $CsPbBr_3$ precursor solution, which endows the prepared film with a better surface coverage with a smoothened surface. Furthermore, it is revealed that inserting a thin PVP nanothick interlayer at the poly(3,4-ethylenedioxythiophene):poly(4-styrenesulfonate) (PEDOT:PSS)/emissive layer interface further promotes the film quality and the performance of the derived LED. It is mainly attributed to three major consequences: (i) reduced grain size of the emissive layer, which facilitates charge recombination, (ii) reduced current leakage due to the enhanced electron-blocking effect, and (iii) improved color purity and air stability owing to better defect passivation. As a result, the optimized composite emissive film can retain the luminescence properties even on exposure to ambient conditions for 80 days and ∼62% of its initial PL intensity can be preserved after 30 days of storage without any encapsulation.

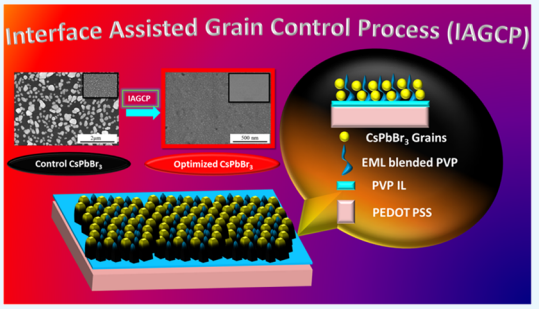

INTRODUCTION

Inorganic perovskite $CsPbBr_3$ holds a tremendous potential in the field of solar cells,[1] field-effect transistors,[2] memory devices,[3] and light-emitting devices.[4−6] $CsPbBr_3$ turns out to be a competitive candidate because of its cost-effectiveness, facile color tunability, narrow full width at half-maximum (FWHM), and high photoluminescence quantum yield (PLQY).[7,8] The major backlogs existing with perovskite light-emitting devices (LEDs) are stability, operational lifetime, and efficiency.[9] The major contributors for such poor stability were its improper morphology, which incurs a high density of grain defects to serve as charge-carrier traps.[10,11] Even though much attention was paid by employing polymeric composites,[12] surface additives,[13,14] small molecular additives,[5,15] surface passivation,[16] and ligand passivation,[17] there is still a wide avenue to improve the perovskite LED credibility. Efficiency loss poses a major threat to the scientific community because of power scarcity and dwindling energy resources. The presence of pinholes and unbalanced charge injection into emissive layers (EMLs) lead to nonradiative recombination, thereby causing efficiency loss.[18,19]

Several polymeric encapsulants provide good morphology and support the smoother EML thin film formation by controlling the crystallization kinetics.[20,21] For example, a Lewis base poly(ethylene glycol) (PEG)-doped $CsPbBr_3$ physically fills the grain boundaries to control the grain size and reduce the nonradiative defect sites. A highly soluble derivative of PEG controls the morphological features and presents many superior luminescent characteristics with improved operational stability.[21] Increasing the PAN matrices into the perovskite emissive layer alters the diffusivity, aids the formation of a continuous compact film, and smoothens the charge-transfer process.[22] Interestingly, Cai et al. fabricated emissive layers with higher surface coverage and lower surface roughness of 3 nm employing a poly(2-ethyl-2-oxazoline) (PEOXA) polymer, which forms coordinate bonds with metallic lead ions.[23] These efforts portray the establishment of a significant role of polymer additive engineered emissive

Received: February 20, 2020
Accepted: March 24, 2020
Published: April 9, 2020

https://dx.doi.org/10.1021/acsomega.0c00758
ACS Omega 2020, 5, 8972−8981

layers in determining the device efficiency and luminescent properties. To improve the efficiency and stability, the emissive layer and the hole-injection layer (HIL) should be compatible to establish the conformal contact and better injection and block properties.

Poly(3,4-ethylenedioxythiophene):poly(4-styrenesulfonate) (PEDOT:PSS) is a commonly used hole-injection layer with the advantages of high transparency, easy fabrication process, high conductivity, good surface morphology, thermal stability, and excellent mechanical flexibility.[24] However, PEDOT:PSS suffers from several drawbacks/limitations such as (i) hygroscopic nature that traps moisture and leads to device instability,[25] (ii) acidic nature that might etch the indium tin oxide (ITO) electrode, inducing the In ion migration,[26] and (iii) energy level misalignment/barriers between PEDOT:PSS and the perovskite emissive layer.[25,27,28] These limitations always contribute to the unstable lifetime and higher turn-on voltage of the perovskite LEDs.

Interlayers were employed for altering the injection and providing good blocking ability to achieve better efficiency and good stability. Following this principle, Koushik et al. incorporated an atomic-layer-deposited Al_2O_3 interlayer between the perovskite emissive layer and PEDOT:PSS, which resulted in a passivation effect and harvested remarkable photovoltaic performance.[29] Similarly, Shi et al. employed a poly-*N*-vinylcarbazole (PVK) layer as a modulating layer on PEDOT:PSS because of its deeper highest occupied molecular orbital (HOMO) level; besides, they further introduced lithium bis(trifluoromethylsulphonyl)imide (Li-TFSI) doping to improve the hole injection.[30] Meanwhile, semimetallic PEDOT:PSS modified with insulating Triton X-100 was shown to effectively block electrons, as evidenced by the reduced leakage current, thereby granting stability to the device.[31] Recently, Kim et al. suppressed the contact barrier between the HIL and emissive layer by employing the composite HIL made of PEDOT:PSS and insulating MoO_3.[3232] Rational comparison between evaporated and solution-processed MoO_3 suggested that the surface roughness of the platform contributes to device deterioration.[33] Meng et al. addressed PEDOT:PSS luminescence quenching and stability issues using solution-processed MoO_3-ammonia-treated PEDOT:PSS.[34]

Several works were performed with Al_2O_3 thin films to improve the electron blocking, thereby enhancing the stability of the device; however, the vapor deposition technique is complicated.[35] Recently, PEDOT:PSS with ammonia graphene oxide was employed to reduce the energy barrier between the injection layer and the emissive layer.[36] From these studies, it is evidenced that the grain size control, surface coverage, and good injection properties without luminescence quenching are essential for designing efficient and stable $CsPbBr_3$ LEDs. As many of the research works represent complex procedures and expensive fabrication, there is still a need for designing a low-cost, eco-friendly facile solution-processing strategy to enhance device efficiency and stability.

Herein, we utilized a low-cost, eco-friendly hydrophilic polymer poly(vinylpyrrolidone) (PVP) to modify the perovskite emissive layer to impart the defect state passivation. We blend PVP into the $CsPbBr_3$ film and use a thin PVP interlayer underlying the emissive layer to prepare a compact pinhole-free emissive layer and enhance the electron-blocking ability, which the conventional PEDOT:PSS could not achieve. We first optimized the $CsPbBr_3$ + 5% PVP blending to achieve a smooth film surface and decent PL characteristics, as evidenced by field emission scanning electron microscopy (FE-SEM), atomic force microscopy (AFM), photoluminescence (PL), and time-resolved photoluminescence (TRPL). Second, we used the optimized $CsPbBr_3$ + 5% PVP emissive layer and the optimal PVP interlayer to achieve the grain size control, higher surface coverage (93%), and better electron-blocking effect. As a result, the PL stability with significantly tripled performance in current efficiency (CE) and external quantum efficiency (EQE, %) is manifested (in comparison with PEDOT:PSS/$CsPbBr_3$ + 5% PVP). Besides, the air stability was improved, for which it maintains the PL emissive characters (62% of its initial value) even under the exposure of ambient room temperature (RT) and 70% relative humidity (RH) for 30 days.

RESULTS AND DISCUSSION

We herein initiated our study with the surface characterizations on the control $CsPbBr_3$ fabricated on the conventional PEDOT:PSS. The first stage process was done on the emissive layer to improve the surface defect passivation and morphological characteristics of $CsPbBr_3$. PVP can act as a good surface modifier, and it controls the perovskite grain growth. The interaction between carbonyl and Pb^{2+} is predominant and effectively reduces the grain defects existing on the surface of pristine perovskite.[37,38] Perovskite embedded within such polymeric matrices can ultimately engender sufficient grain size control. A vast number of polymers have already exhibited good primitive role in controlling the kinetics and morphological features of perovskite. For example, poly(ethylene oxide) (PEO),[19,20] PEG,[21] methoxy PEG,[12] poly(methyl methacrylate) (PMMA),[1] polystyrene (PS),[39] PEOXA,[23] and poly(4-vinylpyridine) (P4VP)[40,41] polymers have been successfully employed in the emissive matrix of perovskite. We herein use the functional polymer PVP for emissive layer modifications because of its nontoxicity, environmental stability, high transparency, solubility, low cost, and facile solution processability.[42] Substrates on which the perovskite is grown act as the major contributor toward the formation of highly ordered perovskite thin films, and they also alter the grain growth rate.[18,25,43] In general, for the common perovskite LEDs, the emissive layers were constructed on top of the PEDOT:PSS layer because of its good hole injection, high conductivity, and high transparency. However, the PEDOT:PSS is hygroscopic and acidic; besides, it has a low work function and UV instability.[18,44] To overcome such inherent limitations, we employ a PVP interlayer onto the PEDOT:PSS surface, which can improve the morphological features, such as grain size and grain defect reduction, of the perovskite film grown on top. It thus can reduce the hole injection to facilitate the charge balance, leading to improved device efficiency. Figure 1a displays the device architecture, where indium tin oxide (ITO) acts as an anode, PEDOT:PSS serves as the hole-injection layer, PVP acts as the (grain-control + hole-control + electron-blocking) interlayer,[45] the perovskite−PVP blend behaves as the emissive layer, 2,2′,2″-(1,3,5-benzinetriyl)-tris(1-phenyl-1-H-benzimidazole) (TPBi) serves as the electron-injection and hole-blocking layer, and LiF/Ag acts as the top cathode. The structure of PVP is given in Figure 1b, and the corresponding energy levels of the device are schematized in Figure 1c, with the published literature values.[5,46,47]

https://dx.doi.org/10.1021/acsomega.0c00758
ACS Omega 2020, 5, 8972−8981

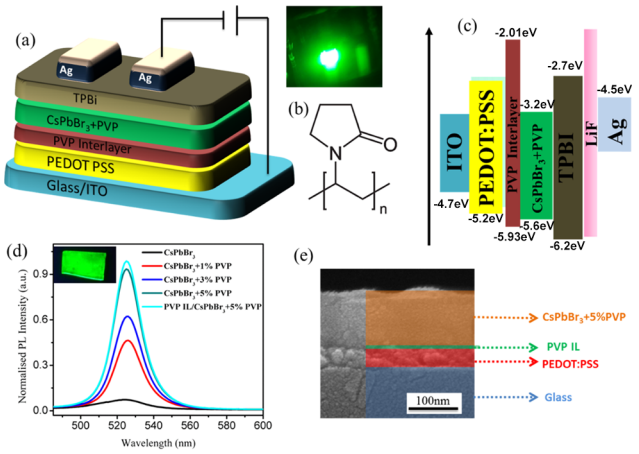

Figure 1. (a) Schematic representation of the LED architecture. (b) Molecular structure of PVP and (c) energy-level diagram of the device. (d) PL intensity diagram of the emissive layers with various PVP weight % and PVP interlayer (IL) and (e) cross-sectional FE-SEM images of the interlayered $CsPbBr_3$ emissive layer.

In this study, we initially optimized the $CsPbBr_3$−PVP blends. Afterward, we further introduced a PVP interlayer modification onto the PEDOT:PSS surface to greatly suppress luminescence quenching, grain size, and surface defects and enhance the electron-blocking effect. In brief, $CsPbBr_3$ was blended with four different weight ratios (1, 3, 5, and 7%) of PVP to optimize the quality of the emissive layer. Steady-state PL measurements revealed PL intensity increment on the PVP blends with the $CsPbBr_3$ matrix and subsequent PVP interlayer modification on PEDOT:PSS (Figure 1d). The bright green luminescence in the inset of Figure 1d proves the emissivity of the PVP interlayered structure, which indirectly states the curtailment of luminescence quenching and improved surface coverage.[48] The FE-SEM cross-sectional image represented in Figure 1e affirms the presence of a PVP interlayer between PEDOT:PSS and the emissive layer, which possibly arrests the excitonic quenching at the PEDOT:PSS interface.

We herein used the facile single spin-coating step to develop a pinhole-free, smooth surface structure due to its simplicity, cost-effectiveness, easy fabrication, and energy-efficient characteristics. Figure 2 shows the FE-SEM images of pure and PVP-blended $CsPbBr_3$ surfaces with a PVP interlayer architecture. Pure $CsPbBr_3$ emissivity hampers the development of light-emitting applications because of the grain surface defects. The pin holes function as electrical shunt paths producing leakage current, which eventually weaken the device efficiency.[35,49] Figure S1 demonstrates the FE-SEM image of pure and PVP-blended $CsPbBr_3$ surfaces without the PVP interlayer architecture. The grain size is large and the surface coverage is low in terms of pure $CsPbBr_3$ developed on the PEDOT:PSS substrate. On varying the blending ratios of PVP from 1 to 5%, the $CsPbBr_3$ grains are confined to a relatively smaller size and the surface coverage is improved to a considerable extent. We suspect that the reason for such grain size reduction and improved surface coverage is the interaction of PVP with Pb^{2+}, which certainly improves the dispersivity of the perovskite precursor.[50,51] The other plausible factor is that the PVP polymer can significantly suppress the diffusivity of the perovskite precursor during film evolution. After the optimum 5% PVP blending, a 7% PVP blend clearly exhibits the agglomeration of $CsPbBr_3$ grains, which is evidenced by Figure S1e due to phase segregation. The grain sizes effectively reduced from several hundred nanometers (~300 nm) to several tens of nanometers (<50 nm) by a PVP interlayer and a PVP-blended emissive layer (Figure 2). In the case of the optimized PVP interlayer/$CsPbBr_3$ + 5% PVP film, the surface coverage was measured to be 93% (using ImageJ software), whereas the surface coverage of the control PEDOT:PSS/$CsPbBr_3$ film was only 41%. The reason for the elevated surface coverage is the dual polymeric encapsulation engendered by the interface-assisted grain control process (IAGCP) (Figure 3c). Figure 3 clearly shows the grain growth comparison on conventional PEDOT:PSS and the PVP interlayer. This controlled grain growth is suspected due to the successful anchoring of PVP blends onto the PVP interlayer/PEDOT:PSS, which eventually contributed to the precise grain growth control.[52] In addition, Figure S4 clearly illustrates the effect of PVP IL modification on the PEDOT:PSS surface. It is worth noting that the PVP IL

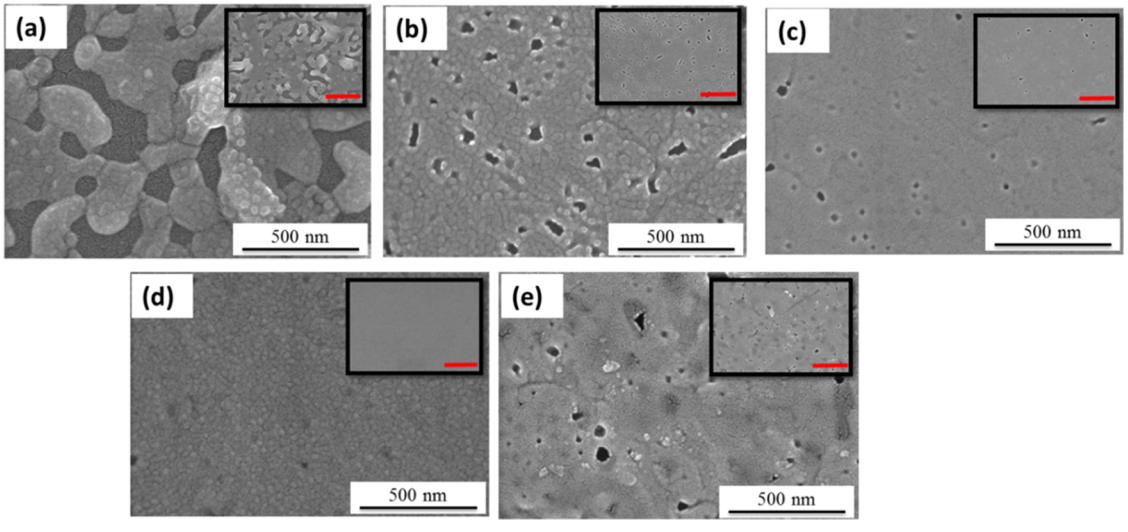

Figure 2. FE-SEM images of (a−e) pure $CsPbBr_3$, $CsPbBr_3$ + 1% PVP, $CsPbBr_3$ + 3% PVP, $CsPbBr_3$ + 5% PVP, and $CsPbBr_3$ + 7% PVP on a PVP interlayer/PEDOT:PSS/glass substrate. Insets correspond to the lower magnification (scale corresponds to 1 μm).

https://dx.doi.org/10.1021/acsomega.0c00758
ACS Omega 2020, 5, 8972−8981

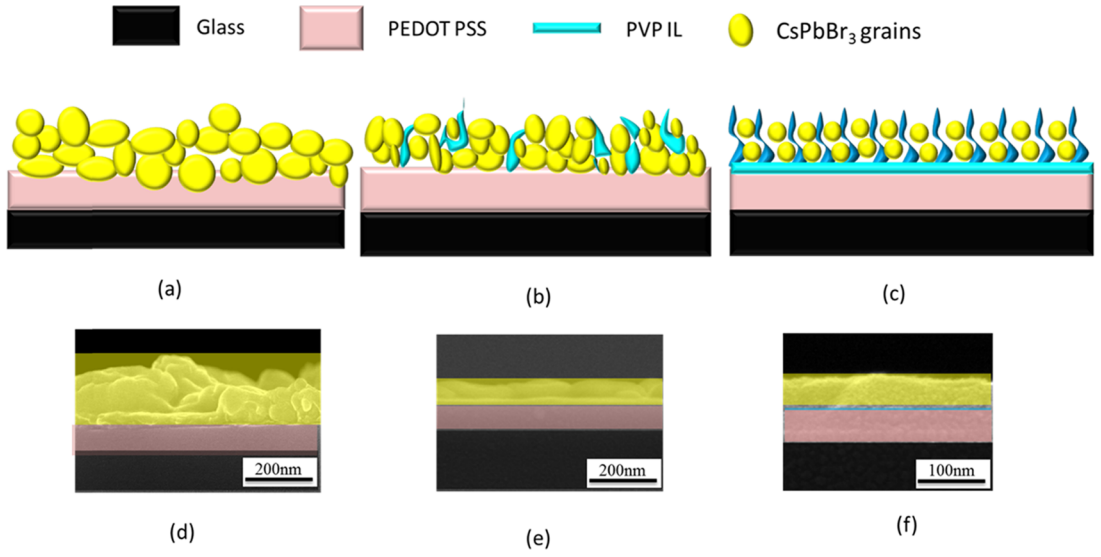

Figure 3. Schematic representation and corresponding FE-SEM images of (a, d) pure $CsPbBr_3$ film spin-coated on PEDOT:PSS/glass, (b, e) $CsPbBr_3$ + 5% PVP film spin-coated on PEDOT:PSS/glass, and (c, f) $CsPbBr_3$ + 5% PVP film spin-coated on PVP interlayer/PEDOT:PSS/glass (IAGCP).

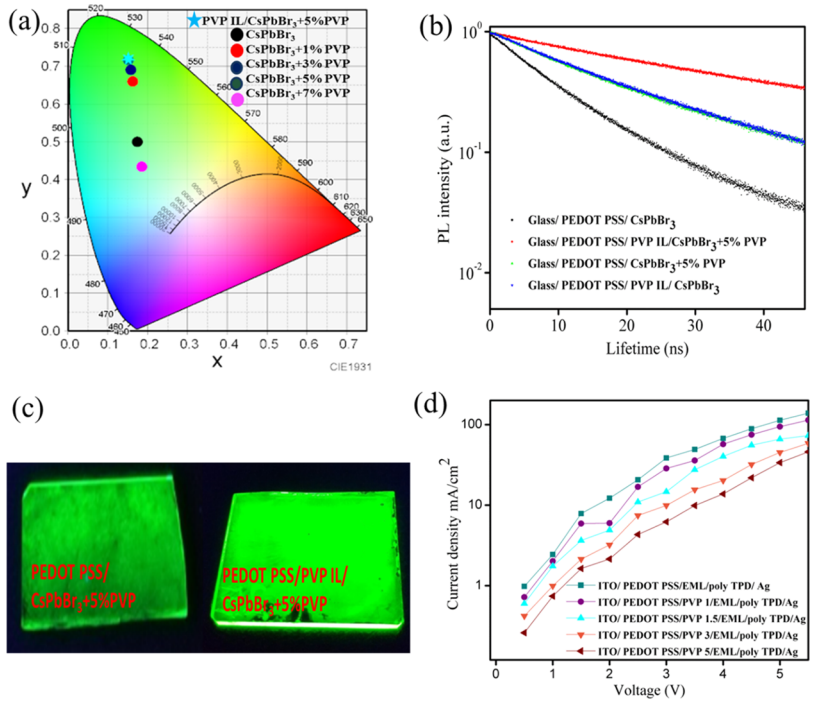

Figure 4. (a) CIE coordinates on PLQY measurements of pure $CsPbBr_3$ and other PVP blends of $CsPbBr_3$. (b) TRPL decay curves of pure $CsPbBr_3$, $CsPbBr_3$ + 5% PVP, and with PVP interlayer. (c) Digital photographs of UV-exposed optimized $CsPbBr_3$ + 5% PVP and PVP interlayer/$CsPbBr_3$ + 5% PVP. (d) Hole-only device injection properties with different PVP IL thicknesses spin-coated on to PEDOT:PSS/ITO/glass.

smoothen platform also contributed to the formation of high-quality EML thin films (Figure 1e).

For LED fabrication, compact smooth thin films and uniform distribution of emissive layers are desirable for harvesting better efficiency.[43] The AFM observations were in agreement with FE-SEM observations, and the root-mean-square surface roughness (R_q) values indirectly complied with FE-SEM results. The smoothness is good in the case of optimized $CsPbBr_3$ + 5% PVP thin film deposited on PEDOT:PSS, and the value is ~3.6 nm, whereas pure $CsPbBr_3$ exhibits a detrimental roughness of 22.4 nm (Figure S2). Utilization of the PVP interlayer significantly reduced the surface roughness to 1.4 nm ($CsPbBr_3$ + 5% PVP), which portrays the development of ultrasmooth compact perovskite thin films. We attribute the morphological changes such as grain size reduction and smoothness to the surface energy changes with a hydrophilic PVP platform[25,37] and the coexisting PVP matrix embedment assisted by the dual polymeric encapsulation. Interestingly, the comparison of AFM images (Figure S5) of PEDOT:PSS (roughness 1.3 nm) and PEDOT:PSS/PVP interlayer (roughness 0.9 nm) also

https://dx.doi.org/10.1021/acsomega.0c00758
ACS Omega 2020, 5, 8972−8981

Table 1. Detailed Decay Parameters of TRPL Measurements

samples	A_1	τ_1 (ns)	A_2	τ_2 (ns)	τ_{avg} (ns)
glass/PEDOT:PSS/$CsPbBr_3$	0.4751	6.5190	0.4780	14.04	11.66
glass/PEDOT:PSS/$CsPbBr_3$ + 5% PVP	0.3689	6.9152	0.6385	36.51	36.24
glass/PEDOT:PSS/PVP IL/$CsPbBr_3$	0.4428	11.8111	0.6440	31.7809	27.19
glass/PEDOT:PSS/PVP IL/$CsPbBr_3$ + 5% PVP	0.3315	14.2507	0.7415	68.6293	64.01

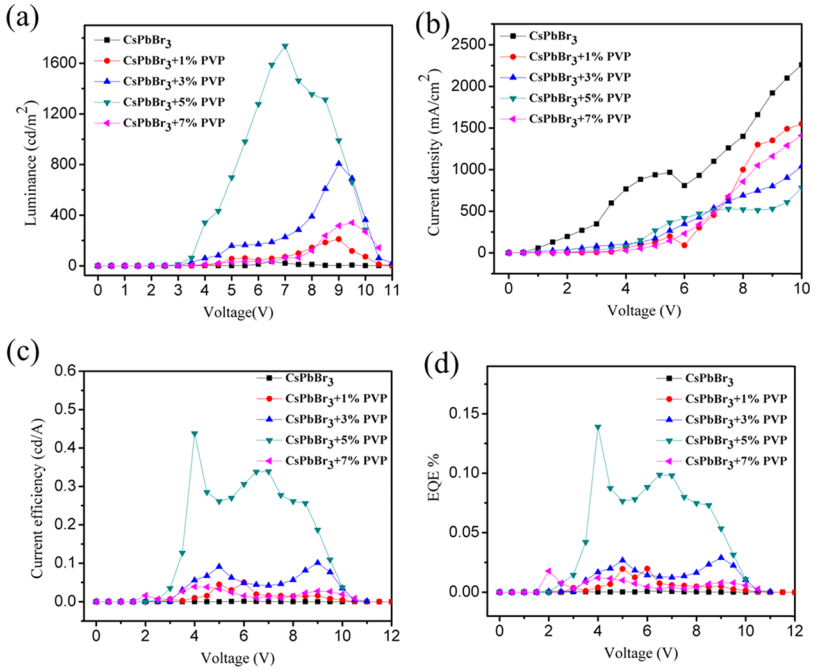

Figure 5. (a) Luminance vs voltage, (b) current density vs voltage, (c) current efficiency vs voltage, and (d) EQE vs voltage of pure $CsPbBr_3$ and PVP-blended emissive layered LED device performance.

ascertains the evolution of ultrasmooth surface characters (Figure S3).

We intend to study the PLQY of the prepared emissive layers, as it influences the device performance considerably.[53] The uniform enhanced surface coverage of grains and defect passivation contributed to the enhanced PLQY of 10.4%, whereas pure perovskite exhibits PLQY of only 0.5%. These PLQY trends are comparable and occur due to the developed surface passivation and exclusive grain control. $CsPbBr_3$ with PVP (0, 1, 3, and 5%) exhibits PLQY values of 0.5, 5.9, 6.5, and 10%, which is a direct indication of better defect passivation. The existence of a PVP interlayer further enhances the PLQY to 10.4%, suggesting the reduced interfacial excitonic quenching between PEDOT:PSS and an emissive layer. The PLQY associated Commission Internationale de I'Eclairage (CIE) coordinate diagram elaborated the ultrapure green color of the emissive layers obtained with various PVP blending and interlayer modifications (Figure 4a), and its green emissive characters followed the PLQY trend.[48,54] The CIE color coordinates are (0.1512, 0.7206) for the optimized PVP interlayer/$CsPbBr_3$ + 5% PVP and (0.1515, 0.7167) for $CsPbBr_3$ + 5% PVP (Figure 4a). The presence of a PVP interlayer thankfully enhanced the PLQY and CIE coordinates to a small extent without altering the PL narrow FWHM of 18 nm, featuring the healthy green emissive characteristics.

To better understand the surface defect passivation and defect state reduction with PVP blended and PVP interlayered, we studied time-resolved PL (TRPL) measurements fitted with a biexponential function (Figure 4b). The decay curve results (Table 1) affirmed the reduced nonradiative recombination of the $CsPbBr_3$ + 5% PVP-blended film as compared to that of the pure $CsPbBr_3$ film. The longer lifetime τ_2 indicates the superior applicability of the PVP interlayer design. Such a long lifetime can be ascribed to the synergistic influence of a compact pinhole-free surface enabled by IAGCP and improved defect passivation, which reduces the nonradiative recombination to grant a high PLQY of 10.4%.[5,53,55] Furthermore, PVP dopants have been already utilized to suppress the contact quenching between the injection and emissive layers, and our result agrees with the previously reported literature.[56] From the above results, it is evident that luminescence quenching is substantially reduced by IAGCP offered by dual polymeric encapsulation.

In addition to steady-state PL and PLQY measurements, images of UV-exposed PEDOT:PSS/$CsPbBr_3$ + 5% PVP and PVP interlayer/PEDOT:PSS/$CsPbBr_3$ + 5% PVP films were captured to provide the real-time visual observation differences (Figure 4c). Additionally, we attempted to study the hole-injection properties of the PVP interlayer with its different concentrations. As concentration has a direct influence on the spin-coated thin films, we utilized different concentrations to alter the thickness of interlayers.[57,58] Recently, most researchers focused on the polymeric blending strategy to alter the PEDOT:PSS work function to achieve a higher HOMO level.[33,44,59] We herein fabricated the hole-only device with a PVP interlayer and monitored the current density under varied applied forward bias. The hole-only device was fabricated with the control PEDOT:PSS and the PVP

https://dx.doi.org/10.1021/acsomega.0c00758
ACS Omega 2020, 5, 8972−8981

Table 2. Device Performance of Pure Perovskite and PVP-Blended Perovskite with Different Ratios

samples	L_{max}@bias (cd/m^2)@V	turn-on voltage (V)	current efficiency (cd/A)@V	EQE (%)@V
$CsPbBr_3$	34@6.5 V	3.0	0.003@6.5 V	0.001@6.5 V
$CsPbBr_3$ + 1% PVP	211@9.0 V	4.0	0.045@5.0 V	0.019@5.0 V
$CsPbBr_3$ + 3% PVP	806@8.0 V	3.0	0.101@9.0 V	0.029@9.0 V
$CsPbBr_3$ + 5% PVP	1737@7.0 V	3.0	0.438@4.0 V	0.139@4.0 V
$CsPbBr_3$ + 7% PVP	340@9.5 V	3.0	0.027@9.0 V	0.080@9.0 V

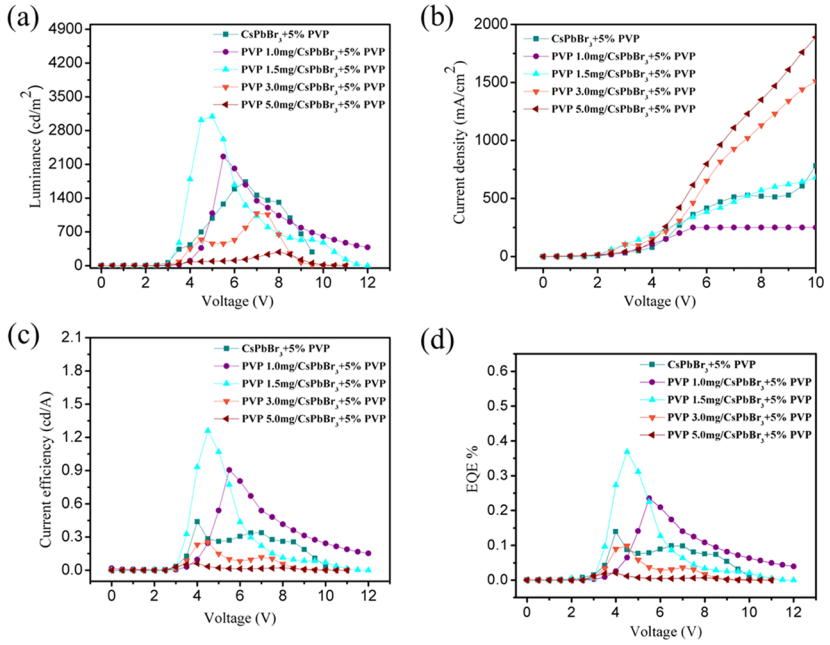

Figure 6. (a) Luminance vs voltage, (b) current density vs voltage, (c) current efficiency vs voltage, and (d) EQE vs voltage of pure $CsPbBr_3$ and PVP-blended emissive layered LED device constructed with the novel thin layered PVP IL surface.

interlayer of different thicknesses, following the architecture of the ITO/PEDOT:PSS/PVP interlayer (x)/$CsPbBr_3$ + 5% PVP/poly-TPD/Ag, where x refers to different concentrations such as 1.0, 1.5, 3.0, and 5.0 mg/mL. The hole-injection results evidence that the 1.5 mg/mL PVP interlayer concentration restricts the hole injection considerably even under the applied voltage of 5 V because of the contact barrier reduction. From Figure 4d, it is evident that 1.5 mg/mL can retard the leakage current and governs the hole injection into the emissive layer, providing a balanced charge-carrier injection with the possible promotion of device efficiency.

After the successful emergence of surface morphological and optical characterization, we extend it to device fabrication. First, we fabricated a set of device with the architecture glass/ITO/PEDOT:PSS/$CsPbBr_3$ + x% PVP/TPBi/LiF/Ag. The current density−voltage (J−V), luminance−voltage (L−V), current efficiency (CE), and external quantum efficiency (EQE) characteristics are displayed in Figure 5, and their corresponding device performance is summarized in Table 2. The control $CsPbBr_3$ device exhibited poor maximum luminance, CE, and EQE of 34 cd/m^2 (at 6.5 V), 0.003 cd/A (at 6.5 V), and 0.001% (at 6.5 V), respectively. This poor performance was apparently due to the improper surface coverage and irregular rough surface. After blending $CsPbBr_3$ with the PVP polymer (0−5%), the luminance, current efficiency, and EQE (%) kept progressing because of the improved morphological features, relatively high coverage, and defect passivation. Table 2 shows that the optimized $CsPbBr_3$ + 5% PVP emissive layer on PEDOT:PSS harvested better luminance, CE, and EQE of 1734 cd/m^2 (7.0 V), 0.438 cd/A (4.0 V), and 0.139% (4.0 V), respectively.

In the second stage, we extended the device fabrication with the first stage optimized $CsPbBr_3$ + 5% PVP emissive layer on our novel PVP interlayer to monitor the influence of its thickness on the resulting device performance. We utilized the simple solution process to alter the thickness of the PVP interlayer and the newly adopted device architecture composed of glass/ITO/PEDOT:PSS/x PVP interlayer/$CsPbBr_3$ + 5% PVP/LiF/Ag. Our architecture is novel and unique (as many of the LEDs follow the architecture of commercially available expensive hole injectors, like PVK and poly-TPD) and such a PVP interlayer is first studied along with a $CsPbBr_3$ + 5% PVP emissive layer to explore the stability and efficiency enhancement. The AFM depth profile analysis was done with various PVP concentrations (1, 1.5, 3.0, and 5.0 mg/mL), and the measured average thicknesses were ∼1, 2, 5, and 10 nm, respectively (Figure S6a−e). (The thickness measurements are briefly given in the Experimental Section; they are performed with five different locations and averaged to get the thickness.) For the optimized PVP interlayer concentration of 1.5 mg/mL, the thickness matches exactly with the FE-SEM cross-sectional image (Figure 1e), proving the reliability of the solution processability of this thin interlayer. The champion PVP 1.5 mg/$CsPbBr_3$ + 5% PVP device outperformed the other devices in terms of luminance, CE, and EQE. The CE (1.26 cd/A) and EQE (0.369%) of the PVP interlayer were tripled in comparison with the conventional PEDOT:PSS HIL (Figure 6 and Table 3). The luminance was almost doubled and EL

https://dx.doi.org/10.1021/acsomega.0c00758
ACS Omega 2020, 5, 8972−8981

Table 3. Performance of PVP Interlayered Devices with Different Thicknesses

samples	L_{max}@bias (cd/m^2)@V	turn-on voltage (V)	current efficiency (cd/A)@V	EQE (%)@V
$CsPbBr_3$ + 5% PVP	1737@7 V	3.0	0.44@4.0 V	0.139@4.0 V
PVP 1.0 mg/$CsPbBr_3$ + 5% PVP	2262@5 V	3.0	0.90@5.5 V	0.235@5.5 V
PVP 1.5 mg/$CsPbBr_3$ + 5% PVP	3094@5 V	3.0	1.26@4.5 V	0.369@4.5 V
PVP 3.0 mg/$CsPbBr_3$ + 5% PVP	1085@7 V	3.0	0.12@7.0 V	0.036@7.0 V
PVP 5.0 mg/$CsPbBr_3$ + 5% PVP	281@8 V	3.0	0.02@8.0 V	0.006@8.0 V

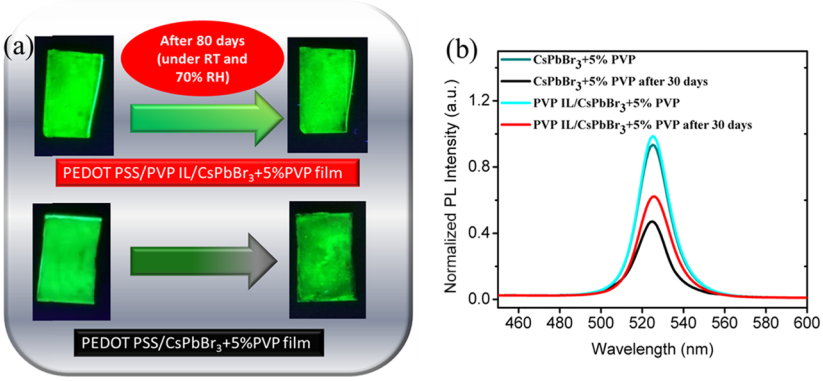

Figure 7. (a) Comparison of photographs of UV-exposed glass/PEDOT:PSS/$CsPbBr_3$ + 5% PVP and glass/PEDOT:PSS/PVP IL/$CsPbBr_3$ + 5% PVP emissive thin films and (b) PL stability curve of the glass/PEDOT:PSS/$CsPbBr_3$ + 5% PVP and the glass/PEDOT:PSS/PVP IL/$CsPbBr_3$ + 5% PVP before and after 30 days.

FWHM was relatively reduced in the case of the PVP interlayer champion device with a low turn-on voltage of 3 V. Our results are comparatively better than those published in the recent literature in terms of current efficiency and EQE (%).[5,27,32,49,60] A lowered turn-on voltage proved that lowered energy level barriers existed between the HIL and emissive layers. Additionally, the color stability and color purity issues were addressed with our novel champion device excelled with the robust emissive characteristics. Figures S7 and S8 contrast the narrowed EL FWHM of 22 nm and stable EL CIE ultrapure green color under lower and maximum bias values.

As our IAGCP strategy engenders dual polymeric encapsulation, we believe that our $CsPbBr_3$ emissive film can retain its emissive characteristics for a prolonged period of time even under room temperature (RT) and higher relative humidity (RH). Figure 7a clearly demonstrates the PL stability of our novel structured emissive layer toward higher RH% even after 80 days. Figure 7b reveals that the PVP interlayer/$CsPbBr_3$ + 5% PVP film retained ∼62% of its initial PL intensity even after 30 days of exposure to RT and 70% RH, whereas the PEDOT:PSS/$CsPbBr_3$ + 5% PVP film retained only ∼50% after the same exposure time. The UV-exposure image clearly rationalized the differences between the novel interlayer-structured and conventional films. Although we did not achieve state-of-the-art values, we developed a novel IAGCP to confine the surface morphological features and thereby increase the device performance and stability cohesively. Our novel IAGCP can be a potential runway for designing stable and pinhole-free perovskite thin films, and further enhancement with the device is desired for the futuristic advanced applications.

CONCLUSIONS

Our proposed IAGCP method can produce 93% compact surface coverage with controlled grain size without any complex expensive toxic ligands or solvents. TRPL and PL stability results strongly corroborate the existence of a low-defect surface, featuring the enhanced radiative recombination process. Our novel PVP interlayer structured champion device manifests greater EL characteristics and ultrapure green color with 3 times increase in CE and EQE as compared to the control PEDOT:PSS/$CsPbBr_3$ + 5% PVP film. In addition, PL stability was relatively high under RT and 70% RH, enabling the wide possible directions in developing scalable, efficient, and stable LEDs. This cost-effective solution-based IAGCP strategy will remain at a forefront, and it will create new opportunities in generating a more advanced and sustainable LED fabrication process.

EXPERIMENTAL SECTION

Materials. Cesium bromide (CsBr, 99%) and lead bromide ($PbBr_2$, 99.99%) were purchased from Alfa Aesar. Patterned indium tin oxide (ITO) glass (sheet resistance of 5 Ω) with dimensions of 30 × 30 × 0.7 mm^3 was purchased from Lumtic. Poly(vinylpyrrolidone) (PVP, M_w = 1 300 000), 2,2′,2″-(1,3,5-benzinetriyl)-tris(1-phenyl-1-H-benzimidazole) (TPBi), LiF, and dimethyl sulfoxide (DMSO, ≥99.9%) were purchased from Sigma-Aldrich. Poly(2,3-dihydrothieno-1,4-dioxin)-poly-(styrenesulfonate) (PEDOT:PSS, AI4803) was purchased from Ossila. All of the materials were directly used without further purification.

Solution Preparation. CsBr and $PbBr_2$ with a molar ratio of 1.8:1 (0.3 M) were first mixed in DMSO and then mixed with PVP in four different weight % (namely, 1, 3, 5, and 7%) to prepare the $CsPbBr_3$ + x% PVP precursor solution. For PVP IL preparation, different concentrations of PVP were made with 1, 1.5, 3.0, and 5.0 mg/mL in dimethylformamide (DMF) solvent.

Film Preparation and Device Fabrication. ITO substrates were sequentially cleaned using deionized water, acetone, and isopropyl alcohol (IPA), followed by ozone treatment for 20 min. After cleaning, a PEDOT:PSS layer

https://dx.doi.org/10.1021/acsomega.0c00758
ACS Omega 2020, 5, 8972−8981

(45−50 nm) was spin-coated onto the ITO glass at 3000 rpm for 60 s and annealed at 130 °C for 15 min. The deposition of perovskite active layer was conducted in a glovebox with the spin-coating process onto PEDOT:PSS at 3000 rpm for 60 s using the prepared precursor solutions. Afterward, TPBi (15.0 nm), LiF (1 nm), and Ag (80 nm) were sequentially deposited onto the perovskite layer through thermal evaporation under 4 × 10^{-6} Torr pressure at deposition rates of 0.3, 0.2, and 1 Å/s to complete the device fabrication (Figure 1a). The active area of our fabricated device is 0.2 × 0.2 cm^2. For IL devices, the as-prepared PVP IL solution was spin-cast onto the PEDOT:PSS at 2000 rpm for 60 s followed by 80 °C annealing prior to depositing the perovskite precursor.

Characterization. The surface morphologies of the films were measured by field emission scanning electron microscopy (FE-SEM, Hitachi S-4700 scanning electron microscope) and AFM (Bruker) in taping mode. The photoluminescence spectra of the prepared perovskite films were measured by Flouromax-4, while the UV−vis absorption spectra were measured by Jasco V-730. The PLQY was measured using an integrated sphere method, and the excitation power density was 3.63 $\mu W/cm^2$. Device's performance including current−voltage, luminescence, current efficiency, EQE, and EL spectra were recorded by a spectrophotometer (PR-670) coupled with Keithley 2400. All of the measurements were conducted in ambient air at room temperature. TR-PL spectra were collected for our samples, which is coupled to a spectrometer (iHR320, HORIBA) with Hamamatsu C10910 streak camera and M10913 slow single sweep unit.

■ ASSOCIATED CONTENT

Supporting Information

The Supporting Information is available free of charge at https://pubs.acs.org/doi/10.1021/acsomega.0c00758.

FE-SEM images of PVP-blended perovskite; AFM images of PVP-blended perovskite and interlayered blended perovskite; FE-SEM and AFM images of PEDOT:PSS and PEDOT:PSS/PVP IL; AFM depth profile images of interlayers; EL and CIE coordinates of the fabricated devices; and EL FWHM comparison plots of the LEDs (PDF)

■ AUTHOR INFORMATION

Corresponding Author

Chi-Ching Kuo − *Institute of Organic and Polymeric Materials, Research and Development Center of Smart Textile Technology, National Taipei University of Technology, 10608 Taipei, Taiwan;* orcid.org/0000-0002-1994-4664; Phone: 886-2-27712171; Email: kuocc@mail.ntut.edu.tw; Fax: 886-2-27317174

Authors

Loganathan Veeramuthu − *Institute of Organic and Polymeric Materials, Research and Development Center of Smart Textile Technology, National Taipei University of Technology, 10608 Taipei, Taiwan*

Fang-Cheng Liang − *Institute of Organic and Polymeric Materials, Research and Development Center of Smart Textile Technology, National Taipei University of Technology, 10608 Taipei, Taiwan; Centre de Recherches sur les Macromolécules Végétales (CERMAV), Grenoble Alpes University, Institut Carnot PolyNat, 38041 Grenoble Cedex 9, France*

Zhi-Xuan Zhang − *Institute of Organic and Polymeric Materials, Research and Development Center of Smart Textile Technology, National Taipei University of Technology, 10608 Taipei, Taiwan*

Chia-Jung Cho − *Institute of Organic and Polymeric Materials, Research and Development Center of Smart Textile Technology, National Taipei University of Technology, 10608 Taipei, Taiwan*

Ender Ercan − *Department of Chemical Engineering and Advanced Research Center for Green Materials Science and Technology, National Taiwan University, 106 Taipei, Taiwan*

Chu-Chen Chueh − *Department of Chemical Engineering and Advanced Research Center for Green Materials Science and Technology, National Taiwan University, 106 Taipei, Taiwan;* orcid.org/0000-0003-1203-4227

Wen-Chang Chen − *Department of Chemical Engineering and Advanced Research Center for Green Materials Science and Technology, National Taiwan University, 106 Taipei, Taiwan;* orcid.org/0000-0003-3170-7220

Redouane Borsali − *Centre de Recherches sur les Macromolécules Végétales (CERMAV), Grenoble Alpes University, Institut Carnot PolyNat, 38041 Grenoble Cedex 9, France;* orcid.org/0000-0002-7245-586X

Complete contact information is available at: https://pubs.acs.org/10.1021/acsomega.0c00758

Author Contributions

‖L.V. and F.-C.L. contributed equally to this work.

Notes

The authors declare no competing financial interest.

■ ACKNOWLEDGMENTS

This work was supported by the Ministry of Science and Technology, Taiwan (grants: MOST 106-2221-E-027-119-MY3, MOST 105-2221-E-027-134-MY3, and MOST 104-2113-M-027-007-MY3).

■ REFERENCES

(1) Tong, J.; Luo, J.; Shi, L.; Wu, J.; Xu, L.; Song, J.; Wang, P.; Li, H.; Deng, Z. Fabrication of highly emissive and highly stable perovskite nanocrystal-polymer slabs for luminescent solar concentrators. *J. Mater. Chem. A* **2019**, *7*, 4872−4880.

(2) Yu, W.; Li, F.; Yu, L.; Niazi, M. R.; Zou, Y.; Corzo, D.; Basu, A.; Ma, C.; Dey, S.; Tietze, M. L.; et al. Single crystal hybrid perovskite field-effect transistors. *Nat. Commun.* **2018**, *9*, No. 5354.

(3) Ercan, E.; Chen, J.-Y.; Shih, C.-C.; Chueh, C.-C.; Chen, W.-C. Influence of polymeric electrets on the performance of derived hybrid perovskite-based photo-memory devices. *Nanoscale* **2018**, *10*, 18869−18877.

(4) Ercan, E.; Tsai, P.-C.; Chen, J.-Y.; Lam, J.-Y.; Hsu, L.-C.; Chueh, C.-C.; Chen, W.-C. Stretchable and ambient stable perovskite/polymer luminous hybrid Nanofibers of multicolor fiber mats and their white LED applications. *ACS Appl. Mater. Interfaces* **2019**, *11*, 23605−23615.

(5) Huang, M.-Y.; Veeramuthu, L.; Kuo, C.-C.; Liao, Y.-C.; Jiang, D.-H.; Liang, F.-C.; Yan, Z.-L.; Borsali, R.; Chueh, C.-C. Improving performance of Cs-based perovskite light-emitting diodes by dual additives consisting of polar polymer and n-type small molecule. *Org. Electron.* **2019**, *67*, 294−301.

(6) Zhang, Q.; Tavakoli, M. M.; Gu, L.; Zhang, D.; Tang, L.; Gao, Y.; Guo, J.; Lin, Y.; Leung, S.-F.; Poddar, S.; et al. Efficient metal halide perovskite light-emitting diodes with significantly improved light extraction on nanophotonic substrates. *Nat. Commun.* **2019**, *10*, No. 727.

(7) Li, Y.; Dai, X.; Chen, D.; Ye, Y.; Gao, Y.; Peng, X.; Jin, Y. Inverted quantum dot light-emitting diodes with conductive interlayers of zirconium acetylacetonate. *J. Mater. Chem. C* **2019**, *7*, 3154−3159.
(8) Tsai, P.-C.; Chen, J.-Y.; Ercan, E.; Chueh, C.-C.; Tung, S.-H.; Chen, W.-C. Uniform Luminous Perovskite Nanofibers with Color-Tunability and Improved Stability Prepared by One-Step Core/Shell Electrospinning. *Small* **2018**, *14*, No. 1870103.
(9) Wang, H.; Sui, N.; Bai, X.; Zhang, Y.; Rice, Q.; Seo, F. J.; Zhang, Q.; Colvin, V. L.; Yu, W. W. Emission recovery and stability enhancement of inorganic perovskite quantum dots. *J. Phys. Chem. Lett.* **2018**, *9*, 4166−4173.
(10) Lin, C. C.; Jiang, D.-H.; Kuo, C.-C.; Cho, C.-J.; Tsai, Y.-H.; Satoh, T.; Su, C. Water-resistant efficient stretchable perovskite-embedded fiber membranes for light-emitting diodes. *ACS Appl. Mater. Interfaces* **2018**, *10*, 2210−2215.
(11) Fu, R.; Zhao, Y.; Li, Q.; Zhou, W.; Yu, D.; Zhao, Q. Enhanced long-term stability of perovskite solar cells by 3-hydroxypyridine dipping. *Chem. Commun.* **2017**, *53*, 1829−1831.
(12) Wu, S.; Zhao, S.; Xu, Z.; Song, D.; Qiao, B.; Yue, H.; Yang, J.; Zheng, X.; Wei, P. Highly bright and stable all-inorganic perovskite light-emitting diodes with methoxypolyethylene glycols modified $CsPbBr_3$ emission layer. *Appl. Phys. Lett.* **2018**, *113*, No. 213501.
(13) Sun, S.-Q.; Hua, X.-C.; Liu, Q.-W.; Wang, T.-T.; Luo, W.; Zhang, Y.-J.; Liao, L.-S.; Fung, M.-K. Influence of a lecithin additive on the performance of all-inorganic perovskite light-emitting diodes. *J. Mater. Chem. C* **2019**, *7*, 2905−2910.
(14) Yoon, S.-S.; Khang, D.-Y. Roles of nonionic surfactant additives in PEDOT:PSS thin films. *J. Phys. Chem. C* **2016**, *120*, 29525−29532.
(15) Yu, F.-X.; Zhang, Y.; Xiong, Z.-Y.; Ma, X.-J.; Chen, P.; Xiong, Z.-H.; Gao, C.-H. Full coverage all-inorganic cesium lead halide perovskite film for high-efficiency light-emitting diodes assisted by 1,3,5-tri(m-pyrid-3-yl-phenyl) benzene. *Org. Electron.* **2017**, *50*, 480−484.
(16) Tavakoli, M. M.; Tavakoli, R.; Yadav, P.; Kong, J. A graphene/ZnO electron transfer layer together with perovskite passivation enables highly efficient and stable perovskite solar cells. *J. Mater. Chem. A* **2019**, *7*, 679−686.
(17) Xiao, Z.; Kerner, R. A.; Zhao, L.; Tran, N. L.; Lee, K. M.; Koh, T.-W.; Scholes, G. D.; Rand, B. P. Efficient perovskite light-emitting diodes featuring nanometre-sized crystallites. *Nat. Photonics* **2017**, *11*, 108.
(18) Ahn, S.; Park, M. H.; Jeong, S. H.; Kim, Y. H.; Park, J.; Kim, S.; Kim, H.; Cho, H.; Wolf, C.; Pei, M.; et al. Fine Control of Perovskite Crystallization and Reducing Luminescence Quenching Using Self-Doped Polyaniline Hole Injection Layer for Efficient Perovskite Light-Emitting Diodes. *Adv. Funct. Mater.* **2019**, *29*, No. 1807535.
(19) Li, J.; Bade, S. G. R.; Shan, X.; Yu, Z. Single-layer light-emitting diodes using organometal halide perovskite/poly (ethylene oxide) composite thin films. *Adv. Mater.* **2015**, *27*, 5196−5202.
(20) Bade, S. G. R.; Li, J.; Shan, X.; Ling, Y.; Tian, Y.; Dilbeck, T.; Besara, T.; Geske, T.; Gao, H.; Ma, B.; et al. Fully printed halide perovskite light-emitting diodes with silver nanowire electrodes. *ACS Nano* **2016**, *10*, 1795−1801.
(21) Song, L.; Guo, X.; Hu, Y.; Lv, Y.; Lin, J.; Liu, Z.; Fan, Y.; Liu, X. Efficient inorganic perovskite light-emitting diodes with polyethylene glycol passivated ultrathin $CsPbBr_3$ films. *J. Phys. Chem. Lett.* **2017**, *8*, 4148−4154.
(22) Ji, X.; Peng, X.; Wang, Q.; Ren, J.; Xiong, Z.; Yang, X. On the performance of polymer: organometal halide perovskite composite light emitting devices: The effects of polymer additives. *Org. Electron.* **2018**, *52*, 350−355.
(23) Cai, W.; Chen, Z.; Li, Z.; Yan, L.; Zhang, D.; Liu, L.; Xu, Q.-h.; Ma, Y.; Huang, F.; Yip, H.-L.; Cao, Y. Polymer-assisted in situ growth of all-inorganic perovskite nanocrystal film for efficient and stable pure-red light-emitting devices. *ACS Appl. Mater. Interfaces* **2018**, *10*, 42564−42572.
(24) Lee, J. H.; Jeong, Y. R.; Lee, G.; Jin, S. W.; Lee, Y. H.; Hong, S. Y.; Park, H.; Kim, J. W.; Lee, S.-S.; Ha, J. S. Highly conductive, stretchable, and transparent PEDOT:PSS electrodes fabricated with triblock copolymer additives and acid treatment. *ACS Appl. Mater. Interfaces* **2018**, *10*, 28027−28035.
(25) Lin, C.; Chen, P.; Xiong, Z.; Liu, D.; Wang, G.; Meng, Y.; Song, Q. Interfacial engineering with ultrathin poly (9, 9-di-n-octylfluorenyl-2, 7-diyl)(PFO) layer for high efficient perovskite light-emitting diodes. *Nanotechnology* **2018**, *29*, No. 075203.
(26) Wang, F.; Xu, Q.; Tan, Za.; Li, L.; Li, S.; Hou, X.; Sun, G.; Tu, X.; Hou, J.; Li, Y. Efficient polymer solar cells with a solution-processed and thermal annealing-free RuO_2 anode buffer layer. *J. Mater. Chem. A* **2014**, *2*, 1318−1324.
(27) Kim, Y. H.; Cho, H.; Heo, J. H.; Kim, T. S.; Myoung, N.; Lee, C. L.; Im, S. H.; Lee, T. W. Multicolored organic/inorganic hybrid perovskite light-emitting diodes. *Adv. Mater.* **2015**, *27*, 1248−1254.
(28) Peng, X.-F.; Wu, X.-Y.; Ji, X.-X.; Ren, J.; Wang, Q.; Li, G.-Q.; Yang, X.-H. Modified conducting polymer hole injection layer for high-efficiency perovskite light-emitting devices: enhanced hole injection and reduced luminescence quenching. *J. Phys. Chem. Lett.* **2017**, *8*, 4691−4697.
(29) Koushik, D.; Verhees, W. J.; Zhang, D.; Kuang, Y.; Veenstra, S.; Creatore, M.; Schropp, R. E. Atomic layer deposition enabled perovskite/PEDOT solar cells in a regular n−i−p architectural design. *Adv. Mater. Interfaces* **2017**, *4*, No. 1700043.
(30) Shi, Y.-L.; Liang, F.; Hu, Y.; Wang, X.-D.; Wang, Z.-K.; Liao, L.-S. High-efficiency quantum dot light-emitting diodes employing lithium salt doped poly (9-vinlycarbazole) as a hole-transporting layer. *J. Mater. Chem. C* **2017**, *5*, 5372−5377.
(31) Shin, D.; Kang, D.; Lee, J.-B.; Ahn, J.-H.; Cho, I.-W.; Ryu, M.-Y.; Cho, S. W.; Jung, N. E.; Lee, H.; Yi, Y. Electronic Structure of Nonionic Surfactant-Modified PEDOT:PSS and Its Application in Perovskite Solar Cells with Reduced Interface Recombination. *ACS Appl. Mater. Interfaces* **2019**, *11*, 17028−17034.
(32) Kim, D. B.; Yu, J. C.; Nam, Y. S.; Kim, D. W.; Jung, E. D.; Lee, S. Y.; Lee, S.; Park, J. H.; Lee, A.-Y.; Lee, B. R.; et al. Improved performance of perovskite light-emitting diodes using a PEDOT:PSS and MoO_3 composite layer. *J. Mater. Chem. C* **2016**, *4*, 8161−8165.
(33) Lee, M. H.; Choi, W. H.; Zhu, F. Solution-processable organic-inorganic hybrid hole injection layer for high efficiency phosphorescent organic light-emitting diodes. *Opt. Express* **2016**, *24*, A592−A603.
(34) Meng, Y.; Ahmadi, M.; Wu, X.; Xu, T.; Xu, L.; Xiong, Z.; Chen, P. High performance and stable all-inorganic perovskite light emitting diodes by reducing luminescence quenching at PEDOT:PSS/Perovskites interface. *Org. Electron.* **2019**, *64*, 47−53.
(35) Li, Z. Enhanced performance of quantum dots light-emitting diodes: The case of Al_2O_3 electron blocking layer. *Vacuum* **2017**, *137*, 38−41.
(36) Feng, S.; Yang, Y.; Li, M.; Wang, J.; Cheng, Z.; Li, J.; Ji, G.; Yin, G.; Song, F.; Wang, Z.; et al. High-performance perovskite solar cells engineered by an ammonia modified graphene oxide interfacial layer. *ACS Appl. Mater. Interfaces* **2016**, *8*, 14503−14512.
(37) Kim, Y. C.; Baek, S.-D.; Myoung, J.-M. Enhanced brightness of methylammonium lead tribromide perovskite microcrystal-based green light-emitting diodes by adding hydrophilic polyvinylpyrrolidone with oleic acid-modified ZnO quantum dot electron transporting layer. *J. Alloys Compd.* **2019**, *786*, 11−17.
(38) Wang, R.; Xue, J.; Wang, K.-L.; Wang, Z.-K.; Luo, Y.; Fenning, D.; Xu, G.; Nuryyeva, S.; Huang, T.; Zhao, Y.; et al. Constructive molecular configurations for surface-defect passivation of perovskite photovoltaics. *Science* **2019**, *366*, 1509−1513.
(39) Kim, M.; Motti, S. G.; Sorrentino, R.; Petrozza, A. Enhanced solar cell stability by hygroscopic polymer passivation of metal halide perovskite thin film. *Energy Environ. Sci.* **2018**, *11*, 2609−2619.
(40) Zuo, L.; Guo, H.; deQuilettes, D. W.; Jariwala, S.; De Marco, N.; Dong, S.; DeBlock, R.; Ginger, D. S.; Dunn, B.; Wang, M.; Yang, Y. Polymer-modified halide perovskite films for efficient and stable planar heterojunction solar cells. *Sci. Adv.* **2017**, *3*, No. e1700106.
(41) Yavari, M.; Mazloum-Ardakani, M.; Gholipour, S.; Tavakoli, M. M.; Taghavinia, N.; Hagfeldt, A.; Tress, W. Reducing Surface

https://dx.doi.org/10.1021/acsomega.0c00758
ACS Omega 2020, 5, 8972−8981

Recombination by a Poly (4-vinylpyridine) Interlayer in Perovskite Solar Cells with High Open-Circuit Voltage and Efficiency. *ACS Omega* **2018**, *3*, 5038−5043.
(42) Lampande, R.; Kim, G. W.; Pode, R.; Kwon, J. H. Effectiveness of a polyvinylpyrrolidone interlayer on a zinc oxide film for interfacial modification in inverted polymer solar cells. *RSC Adv.* **2014**, *4*, 49855−49860.
(43) Zhang, H.; Chen, S. An ZnMgO:PVP inorganic−organic hybrid electron transport layer: towards efficient bottom-emission and transparent quantum dot light-emitting diodes. *J. Mater. Chem. C* **2019**, *7*, 2291−2298.
(44) Wu, S.; Han, S.; Zheng, Y.; Zheng, H.; Liu, N.; Wang, L.; Cao, Y.; Wang, J. pH-neutral PEDOT:PSS as hole injection layer in polymer light emitting diodes. *Org. Electron.* **2011**, *12*, 504−508.
(45) Ahn, Y.; Lee, S.; Kwak, D.-H.; Kim, M.; Kim, D. Y.; Kim, J.; Park, Y.; Suh, M. C. Improving the efficiency of perovskite light emitting diode using polyvinylpyrrolidone as an interlayer. *Appl. Surf. Sci.* **2020**, *507*, No. 145071.
(46) Zhao, F.; Chen, D.; Chang, S.; Huang, H.; Tong, K.; Xiao, C.; Chou, S.; Zhong, H.; Pei, Q. Highly flexible organometal halide perovskite quantum dot based light-emitting diodes on a silver nanowire−polymer composite electrode. *J. Mater. Chem. C* **2017**, *5*, 531−538.
(47) Yu, X.; Yu, X.; Zhang, J.; Zhang, D.; Cai, H.; Zhao, Y. Interfacial modification for improving inverted organic solar cells by poly (N-vinylpyrrolidone). *RSC Adv.* **2015**, *5*, 58966−58972.
(48) Genco, A.; Mariano, F.; Carallo, S.; Guerra, V. L.; Gambino, S.; Simeone, D.; Listorti, A.; Colella, S.; Gigli, G.; Mazzeo, M. Fully Vapor-Deposited Heterostructured Light-Emitting Diode Based on Organo-Metal Halide Perovskite. *Adv. Electron. Mater.* **2016**, *2*, No. 1500325.
(49) Jin, F.; Zhao, B.; Chu, B.; Zhao, H.; Su, Z.; Li, W.; Zhu, F. Morphology control towards bright and stable inorganic halide perovskite light-emitting diodes. *J. Mater. Chem. C* **2018**, *6*, 1573−1578.
(50) Xiong, H.; DeLuca, G.; Rui, Y.; Zhang, B.; Li, Y.; Zhang, Q.; Wang, H.; Reichmanis, E. Modifying perovskite films with polyvinylpyrrolidone for ambient-air-stable highly bendable solar cells. *ACS Appl. Mater. Interfaces* **2018**, *10*, 35385−35394.
(51) Patel, M. H.; Chaudhuri, T. K.; Patel, V. K.; Shripathi, T.; Deshpande, U.; Lalla, N. Dip-coated PbS/PVP nanocomposite films with tunable band gap. *RSC Adv.* **2017**, *7*, 4422−4429.
(52) He, J.; Su, J.; Wang, J.; Zhang, L. Synthesis of water-free PEDOT with polyvinylpyrrolidone stabilizer in organic dispersant system. *Org. Electron.* **2018**, *53*, 117−126.
(53) Chiba, T.; Hoshi, K.; Pu, Y.-J.; Takeda, Y.; Hayashi, Y.; Ohisa, S.; Kawata, S.; Kido, J. High-efficiency perovskite quantum-dot light-emitting devices by effective washing process and interfacial energy level alignment. *ACS Appl. Mater. Interfaces* **2017**, *9*, 18054−18060.
(54) Naphade, R.; Zhao, B.; Richter, J. M.; Booker, E.; Krishnamurthy, S.; Friend, R. H.; Sadhanala, A.; Ogale, S. High Quality Hybrid Perovskite Semiconductor Thin Films with Remarkably Enhanced Luminescence and Defect Suppression via Quaternary Alkyl Ammonium Salt Based Treatment. *Adv. Mater. Interfaces* **2017**, *4*, No. 1700562.
(55) Ling, Y.; Tian, Y.; Wang, X.; Wang, J. C.; Knox, J. M.; Perez-Orive, F.; Du, Y.; Tan, L.; Hanson, K.; Ma, B.; Gao, H. Enhanced Optical and Electrical Properties of Polymer-Assisted All-Inorganic Perovskites for Light-Emitting Diodes. *Adv. Mater.* **2016**, *28*, 8983−8989.
(56) Sun, K.; Li, F.; Zeng, Q.; Hu, H.; Guo, T. Blue quantum dot light emitting diodes with polyvinylpyrrolidone-doped electron transport layer. *Org. Electron.* **2018**, *63*, 65−70.
(57) Zhao, L.; Lee, K. M.; Roh, K.; Khan, S. U. Z.; Rand, B. P. Improved Outcoupling Efficiency and Stability of Perovskite Light-Emitting Diodes using Thin Emitting Layers. *Adv. Mater.* **2019**, *31*, No. 1805836.
(58) Tu, J.; Liu, C.; Fan, Y.; Liu, F.; Chang, K.; Xu, Z.; Li, Q.; Chen, Y.; Li, Z. Enhanced performance and stability of p−i−n perovskite solar cells by utilizing an AIE-active cathode interlayer. *J. Mater. Chem. A* **2019**, *7*, 15662−15672.
(59) Ameen, M. Y.; Pradhan, S.; Suresh, M. R.; Reddy, V. MoO_3 anode buffer layer for efficient and stable small molecular organic solar cells. *Opt. Mater.* **2015**, *39*, 134−139.
(60) Yu, J. C.; Lee, A. Y.; Kim, D. B.; Jung, E. D.; Kim, D. W.; Song, M. H. Enhancing the Performance and Stability of Perovskite Nanocrystal Light-Emitting Diodes with a Polymer Matrix. *Adv. Mater. Technol.* **2017**, *2*, No. 1700003.

https://dx.doi.org/10.1021/acsomega.0c00758
ACS Omega 2020, 5, 8972−8981